Engineering Analysis with Boundary Elements 140 (2022) 607–617

Contents lists available at ScienceDirect

Engineering Analysis with Boundary Elements

journal homepage: www.elsevier.com/locate/enganabound

A novel high-performance quadrature rule for BEM formulations

R. Velázquez-Mata [a], A. Romero [a,*], J. Domínguez [a], A. Tadeu [b,c], P. Galvín [a,d]

[a] Escuela Técnica Superior de Ingeniería, Universidad de Sevilla, Camino de los Descubrimientos, ES-41092, Spain
[b] University of Coimbra, CERIS, Department of Civil Engineering, Pólo II, Rua Luís Reis Santos, 3030-788, Coimbra, Portugal
[c] Itecons, Institute of Research and Technological Development in Construction, Energy, Environment and Sustainability, Rua Pedro Hispano, 3030-289 Coimbra, Portugal
[d] ENGREEN, Laboratory of Engineering for Energy and Environmental Sustainability, Universidad de Sevilla, Camino de los Descubrimientos s/n, ES-41092, Spain

ARTICLE INFO

Keywords:
Boundary integral equation
Singular kernels
Numerical integration
Quadrature
Bernstein polynomials
Bézier curve
General approach
Benchmark problem

ABSTRACT

This paper describes a general approach to compute the boundary integral equations that appear when the boundary element method is applied for solving common engineering problems. The proposed procedure consists of a new quadrature rule to accurately evaluate singular and weakly singular integrals in the sense of the Cauchy Principal Value by an exclusively numerical procedure. This procedure is based on a system of equations that results from the finite part of known integrals, that include the shape functions used to approximate the field variables. The solution of this undetermined system of equations in the minimum norm sense provides the weights of the quadrature rule. A MATLAB script to compute the quadrature rule is included as supplementary material of this work. This approach is implemented in a boundary element method formulation based on the Bézier–Bernstein space as an approximation basis to represent both geometry and field variables for verification purposes. Specifically, heat transfer, elastostatic and elastodynamic problems are considered.

1. Introduction

The Boundary Element Method (BEM) allows to solve several engineering problems such as acoustics scattering, fracture mechanics, soil wave propagation, and heat conduction with high accuracy and efficiency [1]. The BEM is based on the fundamental solution of a particular problem that it is used as the weighting function and allows to eliminate the domain discretization. Then, the methodology results in boundary integral equations (BIE) for a point $\mathbf{x}^*$ located at the arbitrary boundary Γ as follows [2]:

$$c(\mathbf{x}^*)u(\mathbf{x}^*) = \int_\Gamma \left(t(\mathbf{x})\mathcal{G}(\mathbf{x},\mathbf{x}^*) - u(\mathbf{x})\mathcal{H}(\mathbf{x},\mathbf{x}^*) \right) d\Gamma(\mathbf{x}), \tag{1}$$

where $u(\mathbf{x})$ and $t(\mathbf{x})$ are the field variables, $\mathcal{G}(\mathbf{x},\mathbf{x}^*)$ and $\mathcal{H}(\mathbf{x},\mathbf{x}^*)$ are the fundamental solution at point $\mathbf{x}$ due to a point source located at $\mathbf{x}^*$, and the integral-free term $c(\mathbf{x}^*)$ depends only on the boundary geometry at the collocation point $\mathbf{x}^*$. The fundamental solution is chosen according to the actual problem. In addition, the boundary discretization is determined by the fundamental solution.

Eq. (1) allows computing the solution to many problems. The integrals in Eq. (1) can be regular, near-singular, weakly singular, singular or hypersingular integrals, and should be understood in the sense of the Cauchy Principal Value (CPV) or in the Hadamard Finite Part (FP). Regular integrals are integrated by Gaussian quadrature. In the rest of the cases, their analytical evaluation depends on the fundamental solution and the shape functions used to approximate the field variables at the boundary element. Both parameters determine the difficulty of the procedure. Guiggiani [3] discussed and compared several methods of dealing with CPV integrals in BEM. He grouped the methods into two basic approaches, the indirect and direct approaches.

Brebbia and Domínguez [4] proposed an approach to indirectly obtain the second integral on the right-hand side of Eq. (1), once the discretization is done, based on a rigid body motion. However, this approach cannot be used to evaluate the integral involving $\mathcal{G}(\mathbf{x},\mathbf{x}^*)$. Additionally, the regularized BIE where the singularity has been removed by subtracting and adding back terms can be obtained by different techniques. Aliabadi and Hall [5] used a Taylor expansion for the singular integrand that allows to integrate it by numerical quadrature plus an analytical integration, since the singularity is subtracted. Guiggiani and Gigante [6] presented a method for the evaluation of CPV integrals in several dimensions by a transformation that allows for computing the BIE as a sum of regular integrals. The method requires adding some terms to the integral to be evaluated. Karami and Derakhshan [7] also presented an algorithm to evaluate hypersingular integrals based on multiple subtractions and additions to separate singular and regular integral terms. Mukherjee [8,9] and Mukherjee et al. [10] evaluated

* Corresponding author.
E-mail address: aro@us.es (A. Romero).

https://doi.org/10.1016/j.enganabound.2022.04.036
Received 7 March 2022; Received in revised form 12 April 2022; Accepted 26 April 2022
Available online 11 May 2022

the finite parts of singular and hypersingular integrals by a regularization scheme. Recently, Marshall and Richardson [11] have proposed a whole-body regularization to treat the singular integrals that appear in the p-version of the BEM in an efficient and simple way.

Alternatively, direct numerical approaches to compute the BIE have been proposed by quadrature. Telles [12] presented a transformation method applied to the evaluation of singular or near-singular integrals, where the Jacobian of the transformation cancels the singularity. Monegato [13] examined some numerical approaches for the evaluation of one-dimensional and two-dimensional finite-part integrals. Diligenti and Monegato [14] proposed an integration scheme for the implementation of hp-BEM using one-dimensional quadrature formulas with an adequate representation of singular and hypersingular kernels. Later, Monegato and Scuderi [15] constructed rules for the numerical evaluation of integrals of functions that are very smooth everywhere in the domain of integration, except at the boundaries where they possess mild singularities. They proposed a smoothing transformation which allows to numerically compute these integrals. More recently, Monegato [16] described the concept and some main properties of CPV integrals and their application to four examples of engineering problems. Kolm and Rokhlin [17] presented a procedure for the design of high-order quadrature rules for the numerical evaluation of singular and hypersingular integrals in the appropriate finite part sense. Then, Carley [18,19] developed a method for the derivation of quadrature rules suitable for use in BEM, where the integrand has strong singularities up to order two [18] or is near-singular [19] based on Ref. [17]. Boykov et al. [20] developed cubature formulas for evaluating hypersingular integrals based on the direct numerical computation of Hadamard's integrals. Theotokoglou and Tsamasphyros [21] and Tsamasphyros and Theotokoglou [22] proposed numerical quadrature formulas that ensure the exact calculation of singular integrals. Khan et al. [23] presented a methodology for numerical evaluation of CPV of singular integrals with oscillatory Fourier kernel. They applied the algorithm to evaluate the singular integrals on the uniform, scattered, and Chebyshev–Gauss–Lobatto nodes and concluded that the accuracy depends on the nodal distribution.

In previous works, specific developments were done to obtain the CPV of the integrals involving the corresponding problems. In the author's opinion, the power and versatility of the BEM would be strongly exhibited in a methodology that allows to compute the BIE by numerical quadratures for an arbitrary element order. In this case, the application of the BEM for solving common engineering problems is straightforward by a general code where different fundamental solutions are available.

This research describes a procedure that allows to compute the BIE by numerical quadratures. The methodology is based on the computation of weights for the quadrature rules by the solution of an underdetermined system of equations in the minimum norm sense as in Ref. [18]. The equations are obtained from the Cauchy Principal Value of known integrals that include the shape functions evaluated at the quadrature points to increase the accuracy. The proposed method can be used for any element and shape function using only numerical integration. Here, the BEM formulation based on the Bézier–Bernstein space [24] has been implemented to consider, additionally, the exact boundary geometry. Furthermore, this formulation allows the use of arbitrary high-order elements. Bernstein polynomials are accounted for developing this general approach since Lagrange polynomials can be obtained from the Bernstein basis. Discontinuous elements have been considered to simplify the treatment of boundary conditions at boundary discontinuities. The numerical performance of the methodology is validated by its application to potential, elastostatic, elastodynamic, and heat conduction steady-state problems. It can also be used for solving time-dependent problems whose BIEs present the same type of singularity.

The novelties and useful contributions of the work presented herein are: (*i*) numerical quadratures accounting for the element shape functions are suggested for the implementation of the BEM; (*ii*) a `MATLAB` [25] class to compute the quadrature rule is included as supplementary material; (*iii*) the proposed methodology is applied to several BEM fundamental solutions by exclusive numerical integration.

The paper is organized as follows. First, the numerical approach is presented. The quadrature rule to compute the corresponding BIEs is proposed and numerically verified. Next, the BEM formulation in the Bézier–Bernstein space is summarized. Then, the methodology is applied to solve four different problems: (*i*) heat transfer in a hollow cylinder; (*ii*) an acoustic domain with a complex open boundary geometry; (*iii*) the elastostatic behaviour of an annulus with an internal inclusion; and (*iv*) wave scattering in a three-dimensional elastic cylindrical cavity; and the corresponding fundamental solutions are discussed. Finally, the conclusion section summarizes the main contributions of this work.

2. Numerical approach

The starting point for the BEM formulation is the BIE (Eq. (1)). The meaning of the field variables depends on the formulation of the physical problem under study. Once the boundary is discretized into N elements, $\Gamma = \bigcup_{j=1}^{N} \Gamma^j$, and the field variables within an element Γ^j are approximated from the nodal values u^i and t^i through the element shape functions $\phi^i(\mathbf{x})$ of order p, Eq. (1) is rewritten as follows:

$$c(\mathbf{x}^*)u(\mathbf{x}^*) = \sum_{j=1}^{N}\sum_{i=0}^{p}\left[\left(\int_{\Gamma^j}\phi^i(\mathbf{x})\mathcal{G}(\mathbf{x},\mathbf{x}^*)\,d\Gamma\right)t^i - \left(\int_{\Gamma^j}\phi^i(\mathbf{x})\mathcal{H}(\mathbf{x},\mathbf{x}^*)\,d\Gamma\right)u^i\right] \tag{2}$$

A key issue in the BEM is the element integration in Eq. (2). The boundary element formulation for common engineering problems uses Green's function based on the solution of the Laplace equation (heat transfer), Poisson equation (electrostatic), Helmholtz equation (acoustics), or the Cauchy's first law of motion (elasticity and wave propagation in solids), among others. These functions usually have a singularity when the distance r between the collocation point $\mathbf{x}^*$ and the observation point $\mathbf{x}$ points goes to zero. The singularities are of the type of $\log(r)$ and $1/r$ in the cases considered in this paper, and lead to weakly singular and singular element integrations that should be handled properly. Although the logarithmic singularity can be integrated by quadratures, such as those proposed in Ref. [15], the other type must be interpreted as the CPV. A new quadrature rule to assess the singular integral is presented in the following section.

2.1. Quadrature rules

The quadrature rules proposed herein are valid for the weakly singular and singular integrals mentioned above. The proposed method is based on the works of Kolm and Rokhlin [17] and Carley [18]. These authors derived a numerical quadrature for singular and hypersingular integrals based on the Legendre expansion of the element shape function. Here, a new procedure is proposed to generalize the quadrature to adapt it to any BEM formulation. The Lagrange interpolant derived from the Bernstein polynomials was chosen instead of the Legendre expansion to represent the element shape functions. This allows the use of different types of elements in the BEM [24] such as equidistant nodes, Legendre–Gauss–Lobatto (LGL) integration points used in the spectral formulations [26], or simpler distributions such as the family of Chebyshev points. Furthermore, the proposed method is valid for problems with singular integrals such as heat transfer, acoustics, elasticity, and wave propagation in solids, both for two-dimension or two-and-a-half dimensions.

The generality of the proposed method is achieved because of the element shape functions of order p can be derived from the Bernstein basis as [24]:

$$\phi^i(t) = \sum_{k=0}^{n} c_k^i B_k^n(t), \quad i = 0, \dots, p \tag{3}$$

where c_k^i are control points and $B_k^n(t)$ is the Bernstein polynomial of order n defined over the interval $t \in [0, 1]$ as:

$$B_k^n(t) = \binom{n}{k} t^k (1-t)^{n-k}, \quad k = 0, \dots, n \tag{4}$$

Note that the change of variable $t = (\xi + 1)/2$ allows to relate the univariate basis t with the natural coordinate $\xi \in [-1, 1]$. The Lagrange interpolant derived from the Bernstein basis must fulfil the following condition for the shape function ϕ^i at element nodes t_j:

$$\phi^i(t_j) = \sum_{k=0}^{n} c_k^i B_k^n(t_j) = \delta_{ij}, \qquad j = 0, \dots, n \tag{5}$$

where δ_{ij} is the Kronecker delta.

This condition is commonly expressed as a linear system of equations through the Bernstein–Vandermonde matrix $A_{jk} = B_k^n(t_j)$ as follows:

$$\begin{bmatrix} B_0^n(t_0) & B_1^n(t_0) & \dots & B_k^n(t_0) & \dots & B_n^n(t_0) \\ B_0^n(t_1) & B_1^n(t_1) & \dots & B_k^n(t_1) & \dots & B_n^n(t_1) \\ \dots & & & & & \\ B_0^n(t_j) & B_1^n(t_j) & \dots & B_k^n(t_j) & \dots & B_n^n(t_j) \\ \dots & & & & & \\ B_0^n(t_n) & B_1^n(t_n) & \dots & B_k^n(t_n) & \dots & B_n^n(t_n) \end{bmatrix} \begin{Bmatrix} c_0^i \\ c_1^i \\ \dots \\ c_k^i \\ \dots \\ c_n^i \end{Bmatrix} = \begin{Bmatrix} 0 \\ 0 \\ \dots \\ 1 \\ \dots \\ 0 \end{Bmatrix}. \tag{6}$$

Thus, the element shape function $\phi^i(t)$ is defined by the control points obtained from the solution of Eq. (6).

Once the shape function is defined in the Bernstein basis (Eq. (5)), the element integration in Eq. (2) can be rewritten as follows in natural coordinates:

$$\begin{aligned} \int_{-1}^{1} \phi^i(\xi) \mathcal{F}(\xi, \mathbf{x}^*) \frac{d\Gamma}{d\xi} d\xi &= \int_0^1 \phi^i(t) \mathcal{F}(t, \mathbf{x}^*) \frac{d\Gamma}{d\xi} \frac{d\xi}{dt} dt \\ &= \int_0^1 \left(\sum_{k=0}^{n} c_k^i B_k^n(t) \right) \mathcal{F}(t, \mathbf{x}^*) \frac{d\Gamma}{d\xi} \frac{d\xi}{dt} dt \\ &= \sum_{k=0}^{n} c_k^i \left(\int_0^1 B_k^n(t) \mathcal{F}(t, \mathbf{x}^*) \frac{d\Gamma}{d\xi} \frac{d\xi}{dt} dt \right) \end{aligned} \tag{7}$$

where, $\mathcal{F}(t, \mathbf{x}^*)$ stands for the type of singularity in the fundamental solution.

The quadrature rule should be able to compute the last integrals in Eq. (7) accounting for the following singular terms $B_k^n(t)\mathcal{F}(t, \mathbf{x}^*)$ derived from the fundamental solution or its series expansion:

$$\int_{-1}^{1} B_k^n(\xi)\, d\xi = \int_0^1 B_k^n(t) \frac{d\xi}{dt} dt \tag{8}$$

$$\int_{-1}^{1} B_k^n(\xi) \log|\xi^* - \xi|\, d\xi = \int_0^1 B_k^n(t) \log|\xi^* - 2t + 1| \frac{d\xi}{dt} dt \tag{9}$$

$$\text{CPV} \int_{-1}^{1} \frac{B_k^n(\xi)}{\xi^* - \xi} d\xi = \text{CPV} \int_0^1 \frac{B_k^n(t)}{\xi^* - 2t + 1} \frac{d\xi}{dt} dt \tag{10}$$

where, ξ^* is the element natural coordinate of the collocation point $\mathbf{x}^*$, and $\mathcal{F}(\xi, \mathbf{x}^*)$ equals 1, $\log|\xi^* - \xi|$ and $1/(\xi^* - \xi)$, in Eqs. (8)–(10), respectively. Thus, the quadrature rule of order M should approximate these integrals as:

$$\int_{-1}^{1} B_k^n(\xi) \mathcal{F}(\xi, \mathbf{x}^*)\, d\xi = \int_0^1 B_k^n(t) \mathcal{F}(t, \mathbf{x}^*) \frac{d\xi}{dt} dt \simeq \sum_{m=0}^{M} B_k^n(t_m) \mathcal{F}(t_m, \mathbf{x}^*) \frac{d\xi}{dt} w_m \tag{11}$$

where t_m and w_m are the integration points and weights, respectively.

Eqs. (8)–(10) and Eq. (11)), the last one evaluated as an equality, allow to define a system of $3(n+1)$ equations with $M+1$ unknowns that represent the weights w_m of the quadrature rule. The number of equations is given by the three types of integrals and the $n+1$ polynomials, and each equation is related to the integrals defined in Equations (8)–(10) for the Bernstein polynomial $B_k^n(t)$. Then, the following system of equations is obtained:

$$\begin{bmatrix} \psi_0(t_0, \xi^*) & \psi_0(t_1, \xi^*) & \dots & \psi_0(t_m, \xi^*) & \dots & \psi_0(t_M, \xi^*) \\ \psi_1(t_0, \xi^*) & \psi_1(t_1, \xi^*) & \dots & \psi_1(t_m, \xi^*) & \dots & \psi_1(t_M, \xi^*) \\ \dots & & & & & \\ \psi_k(t_0, \xi^*) & \psi_k(t_1, \xi^*) & \dots & \psi_k(t_m, \xi^*) & \dots & \psi_k(t_M, \xi^*) \\ \dots & & & & & \\ \psi_n(t_0, \xi^*) & \psi_n(t_1, \xi^*) & \dots & \psi_n(t_m, \xi^*) & \dots & \psi_n(t_M, \xi^*) \end{bmatrix} \begin{Bmatrix} w_0 \\ w_1 \\ \dots \\ w_m \\ \dots \\ w_M \end{Bmatrix} = \begin{Bmatrix} m_0 \\ m_1 \\ \dots \\ m_k \\ \dots \\ m_n \end{Bmatrix} \tag{12}$$

where,

$$\psi_k(t_m, \xi^*) = \begin{bmatrix} B_k^n(t_m) \dfrac{d\xi}{dt} \\ B_k^n(t_m) \log|\xi^* - 2t_m + 1| \dfrac{d\xi}{dt} \\ \dfrac{B_k^n(t_m)}{\xi^* - 2t_m + 1} \dfrac{d\xi}{dt} \end{bmatrix} \tag{13}$$

$$m_k = \begin{Bmatrix} \int_0^1 B_k^n(t) \dfrac{d\xi}{dt} dt \\ \int_0^1 B_k^n(t) \log|\xi^* - 2t + 1| \dfrac{d\xi}{dt} dt \\ \text{CPV} \int_0^1 \dfrac{B_k^n(t)}{\xi^* - 2t + 1} \dfrac{d\xi}{dt} dt \end{Bmatrix} \tag{14}$$

The generalized moments m_k in Eq. (14) can be obtained from the Brandaõ approach to the finite part integrals [27] according to Ref. [18], and are found in Appendix A. The system of Eqs. (12) is solved in the least-squares sense when overdetermined and in the minimum norm least-squares sense when undetermined. The Jacobian $d\xi/dt$ in Eq. (11) is included in the integration weights to use the integration points ξ_m defined in the interval $[-1, 1]$ which is more appropriate for the BEM formulation.

2.1.1. Numerical verification

Following, the accuracy of the proposed quadrature is discussed in detail. First, the quadrature rule is verified for a discontinuous element of order $p = 4$ defined at Chebyshev points of the first kind and, later, a more elaborate convergence analysis is carried out with different element families and orders.

The element of order $p = 4$ defines the Chebyshev points of the first kind in natural coordinates at $\xi = \{\pm 0.951, \pm 0.587, 0\}$. Fig. 1 shows the integral kernels $\psi_k^n(t, \xi^*)$ used for the design of the quadrature rule when the collocation point is $\xi^* = 0$. The first type of integrand corresponds to the Bernstein basis of order $n = 4$, and the other two are the product of the Bernstein basis by the types of singularities considered in this work (including the Jacobian $d\xi/dt = 2$). A singularity is observed at $t = 0.5$ corresponding to the collocation point $\xi^* = 0$.

Once the integration weights are obtained from Eq. (12), the quadrature rule is verified by the integration of the following integrals:

$$I_0 = \int_{-1}^{1} \varphi_0^i(\xi, \xi^*)\, d\xi = \int_{-1}^{1} \phi^i(\xi)\, d\xi \tag{15}$$

$$I_1 = \int_{-1}^{1} \varphi_1^i(\xi, \xi^*)\, d\xi = \int_{-1}^{1} \phi^i(\xi) \log|\xi^* - \xi|\, d\xi \tag{16}$$

$$I_2 = \text{CPV} \int_{-1}^{1} \varphi_2^i(\xi, \xi^*)\, d\xi = \text{CPV} \int_{-1}^{1} \frac{\phi^i(\xi)}{\xi^* - \xi} d\xi \tag{17}$$

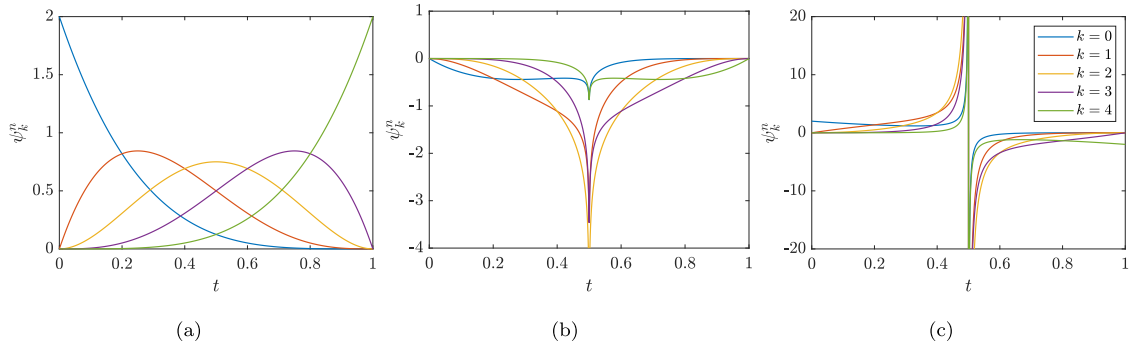

Fig. 1. Integral kernels $\psi_k^n(t, \xi^*)$ for $n = 4$ and $\xi^* = 0$: (a) $B_k^n(t)\dfrac{d\xi}{dt}$, (b) $B_k^n(t)\log|\xi^* - 2t + 1|\dfrac{d\xi}{dt}$, and (c) $\dfrac{B_k^n(t)}{\xi^* - 2t + 1}\dfrac{d\xi}{dt}$.

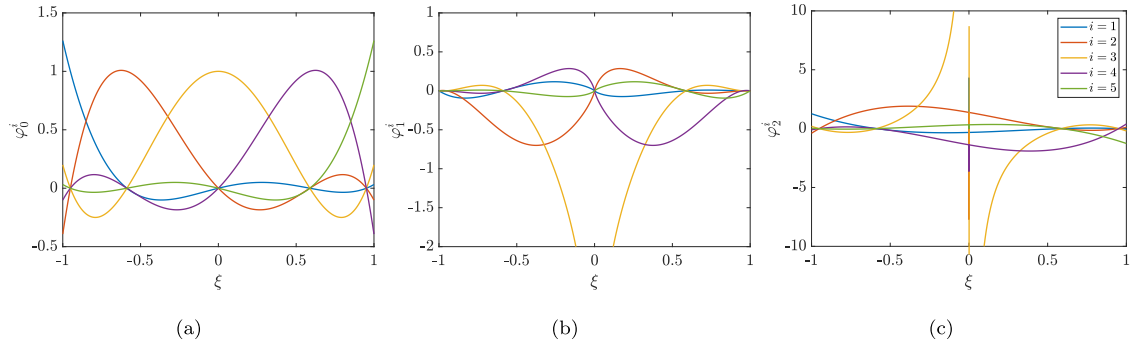

Fig. 2. Integral kernels for Chebyshev points of the first kind, order $p = 4$ and $\xi^* = 0$.

The exact values of these integrals can be computed from the generalized moments in Eq. (14) according to Eq. (7). The control points in Eq. (7) are given by the definition of the shape function in the Bernstein basis.

Fig. 2 shows the integrands in Eqs. (15)–(17) for Chebyshev points of the first kind, order $p = 4$ and $\xi^* = 0$. The integrands in Eqs. (16)–(17) present a singularity at $\xi = 0$ for the shape function with value non-zero at ξ^*. Table 1 summarizes the computed integral values for the five shape functions corresponding to the order $p = 4$. The integrals are numerically evaluated by the proposed approach and using the built-in `integral` MATLAB function [25], and are compared with the exact values computed from Eqs. (7), (14). In the case of Eqs. (15) and (16), the integrals are evaluated accurately by both methods, since regular and weak-singular functions are considered. However, Eq. (17) is only correctly evaluated in the sense of the CPV for the proposed methodology. Moreover, the time consumption using an Intel Core i7-8650U processor at 1.9 GHz were 0.29 ms, 0.66 ms and 0.97 ms using the proposed approach, and 6.0 ms, 41 ms and 43 000 ms using the built-in `integral` MATLAB function, for the Eqs. (15), (16) and (17), respectively. The proposed approach allows to compute the CPV of the considered singular integral in an efficient way. However, `integral` cannot obtain the CPV of the singular integral using a global adaptive quadrature. In this case, MATLAB reached the limit on the maximum number of intervals in use without getting the requested accuracy.

Finally, a convergence analysis is carried out with different element families and orders. Fig. 3 shows the L_2 scaled error ϵ_2 in the computation of integral in Eqs. (15)–(17) for different element order and point distributions: (*i*) Chebyshev points of the first kind; (*ii*) Chebyshev points of the second kind; (*iii*) LGL integration points; and (*iv*) equidistant nodes [24]. The accuracy of the proposed quadrature rules is analysed for different number of integration points M according to the shape function of order p. The quadrature rule did not give accurate results for $M = 2(p + 1)$ and, therefore, this number of integration points is not enough. The integration error increases with the element order p, and is slightly affected by the number of integration points for $M \geq 4(p+1)$. This analysis allows to conclude that a quadrature rule of order $4(p+1)$ is adequate to solve accurately the singular integrals that result from the BEM for solving the engineering problems considered in this paper.

A MATLAB script to compute the quadrature rule is available as supplementary material of this work.[1]

2.2. The BEM formulation in the Bézier–Bernstein space

The BEM formulation in the Bézier–Bernstein space [24,28] is used in this work to show the performance of the proposed quadrature rule. It is based on the application of polynomials in Bernstein form for the definition of Bézier curves $\mathbf{r}_n(t)$:

$$\mathbf{r}_n(t) = \sum_{k=0}^{n} \mathbf{b}_k B_k^n(t) \tag{18}$$

where $\mathbf{b}_k$ are the control points used to approximate the geometry and n is the curve degree. An efficient curve computation is achieved using the polar form (or blossom) of a Bézier curve $\mathbf{r}_n(t)$ [29], which defines a multi-affine transformation satisfying:

$$\mathbf{b}_k = \mathbf{R}(\underbrace{0, \ldots, 0}_{n-k}, \underbrace{1, \ldots, 1}_{k}) \tag{19}$$

where $\mathbf{R}(t_1, \ldots, t_n)$ is computed as:

$$\mathbf{R}(t_1, \ldots, t_n) = \sum_{\substack{I \cap J = \emptyset \\ I \cup J = \{1,2,\ldots,n\}}} \prod_{i \in I}(1 - t_i) \prod_{j \in J} t_j \mathbf{b}_{|J|} \tag{20}$$

[1] http://personal.us.es/pedrogalvin/queen.en.html

Table 1
Computed integral values in Eqs. (15)–(17) for shape functions ϕ^i of order $p = 4$ defined at Chebyshev points of the first kind and $\xi^* = 0$: (*i*) evaluate by the proposed approach (Q), (*ii*) using the built-in `integral` MATLAB function (I), and (*iii*) exact values (Eqs. (7), (14)) (M). The values corresponding to the shape function that presents a non-zero value at $\xi = \xi^*$ are highlighted in grey.

i	M_0	Q_0	I_0	M_1	Q_1	I_1	M_2	Q_2	I_2
0	0.167781	0.167781	0.167781	−0.003188	−0.003188	−0.003188	−0.022868	−0.022868	−0.022868
1	0.525552	0.525552	0.525552	−0.313256	−0.313256	−0.313256	1.738304	1.738304	1.738304
2	0.613333	0.613333	0.613333	−1.367111	−1.367111	−1.367111	−0.000000	−0.000000	−0.633431
3	0.525552	0.525552	0.525552	−0.313256	−0.313256	−0.313256	−1.73804	−1.738304	−1.738304
4	0.167781	0.167781	0.167781	−0.003188	−0.003188	−0.003188	0.022868	0.022868	0.022868

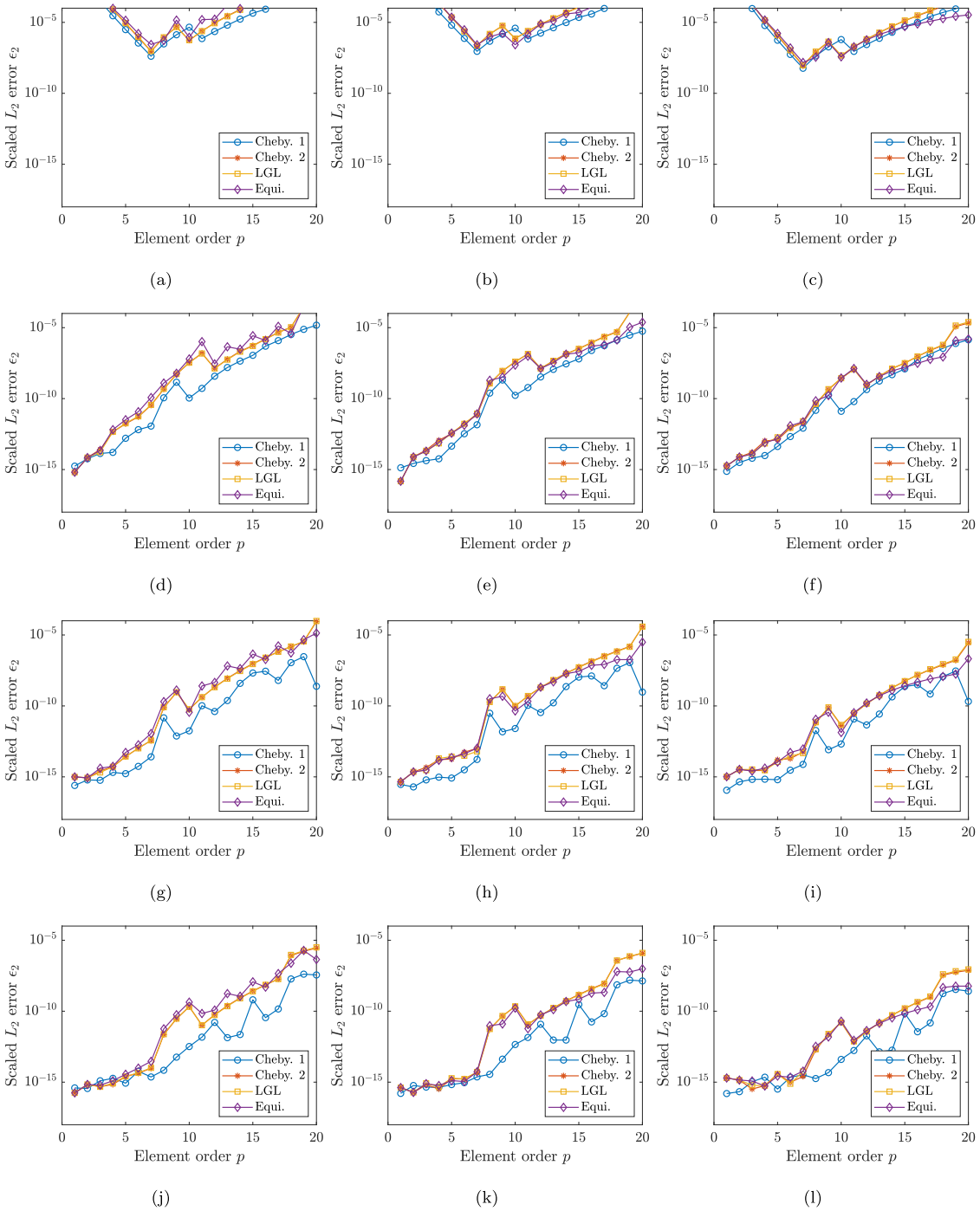

Fig. 3. L_2 scaled error ϵ_2 in the computation of integrals (a,d,g, (j) I_0, (b,e,h, (k) I_1, and (c,f,i, (l) I_2 using (a-c) $M = 2(p+1)$, (d-f) $M = 3(p+1)$, (g-i) $M = 4(p+1)$ and (j-l) $M = 8(p+1)$ integration points.

Thus, a polynomial in Bernstein form can be formulated in the polar form, substituting Eq. (19) into Eq. (18) as follows:

$$\mathbf{r}_n(t) = \sum_{k=0}^{n} \mathbf{R}(\underbrace{0,\dots,0}_{n-k},\underbrace{1,\dots,1}_{k}) B_k^n(t) = \mathbf{R}(t,\dots,t) \tag{21}$$

The Bézier–Bernstein space is used to describe the exact element geometry as $\Gamma^j(\mathbf{x}) = \mathbf{r}_n^j(t)$. Hence, the element integrals in Eq. (2) are rewritten in the univariate basis $t \in [0,1]$ as [24,30]:

$$\int_{\Gamma^j} f(\mathbf{x},\mathbf{x}^*)\, d\Gamma = \int_0^1 f(\mathbf{x}(t),\mathbf{x}^*) \left| \frac{d\mathbf{r}_n^j(t)}{dt} \right| dt \tag{22}$$

where $f(\mathbf{x},\mathbf{x}^*)$ represents the integration kernel. Additionally, Eq. (22) can be transformed into the integration interval $[-1,1]$ to employ the proposed quadrature rule.

The BEM formulation in the Bézier–Bernstein space employs the Lagrange interpolant relative to the Bernstein basis for the field variable approximation to an element [31]. The field approximation given by the shape function interpolates $(n+1)$ nodal values through the element shape functions ϕ^i of order n, for $i = 0,\dots,n$ (Eq. (3)). Then, the field approximation becomes:

$$u(t) = \sum_{i=0}^{p} \phi^i(t) u^i = \sum_{i=0}^{p} \left\{ \sum_{k=0}^{n} c_k^i B_k^n(t) \right\} u^i = \sum_{i=0}^{p} R^i(t,\dots,t) u^i, \tag{23}$$

where the evaluation of the element shape function $\phi^i(t)$ also benefits from the computational advantages of using the polar form $R^i(t_1,\dots,t_n)$ according to Eq. (20). Once the geometry and the field approximation given by Eqs. (21) and (23) are introduced in Eq. (2), the boundary integrals are computed using a standard Gauss–Legendre quadrature with $(p+1)$ integration points whenever the collocation point is sufficiently distant from the integration element. Otherwise, the solution of singular or weakly singular integrals is numerically computed using the proposed quadrature rule.

3. Benchmark problems

The proposed approach is applied to several benchmark problems involving the corresponding fundamental solutions in the BIEs.

3.1. Heat transfer in a two-dimensional hollow cylinder

A hollow cylinder with inner radius $R_1 = 0.4\,\text{m}$ and outer radius $R_2 = 0.7\,\text{m}$ subjected to internal and external temperatures $T_1 = 18\,°\text{C}$ and $T_2 = 0\,°\text{C}$, respectively, was solved to validate the proposed method. The material was characterized by a thermal conductivity of $\lambda = 0.16\,\text{W}\,°\text{C}^{-1}\text{m}^{-1}$.

The exact temperature distribution in the cylinder for a steady-state condition is given by [32]:

$$T(R) = \frac{T_1 - T_2}{\ln(R_1/R_2)} \ln\left(\frac{R}{R_2}\right) + T_2 \tag{24}$$

where R is the distance from the center axis of the cylinder.

Since the geometry is symmetric, only a quarter of the section was discretized. Four patches were used to define the two-dimensional boundary geometry with the control polygon presented in Fig. 4. The inner and outer boundaries were approximated by cubic Bézier curves. The patches were discretized into elements with a maximum length of $h = 0.1\,\text{m}$ and order $p = 6$. A fine grid of internal points equally spaced $0.005\,\text{m}$ was defined.

Dirichlet and Neumann conditions were prescribed on curved and straight boundaries [28], respectively: known temperature on the inner and outer sides of the cylinder and zero heat flow on the symmetry axis.

The Green's function for temperature in an unbounded domain due to concentrated load at $\mathbf{x}^*$ is [4]:

$$\mathcal{G}(\mathbf{x},\mathbf{x}^*) = \frac{1}{2\pi\lambda} \log\left(\frac{1}{r}\right) \tag{25}$$

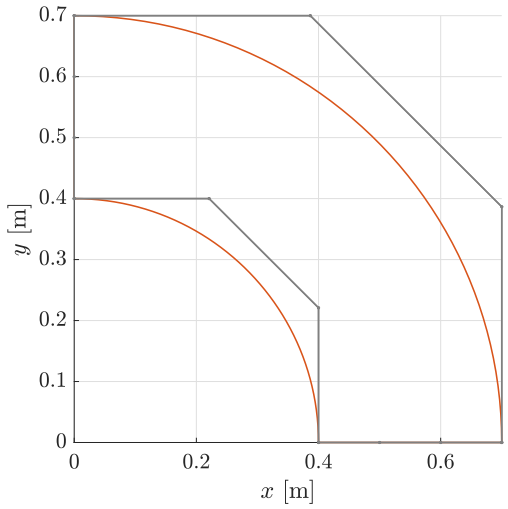

Fig. 4. Boundary geometry of a hollow cylinder (red line) and their related control polygons (grey line). (For interpretation of the references to colour in this figure legend, the reader is referred to the web version of this article.)

In this problem, the variables u^i and t^i in the BIE (Eq. (2)) represent the temperature and heat flux, respectively. The Green's function presents a logarithmic singularity at $r = 0$ that can be handled by the proposed quadrature. The fundamental solution $\mathcal{H}(\mathbf{x},\mathbf{x}^*)$ is obtained by differentiating the Green's function, which increases the order of the singularity by one, and, therefore, the integrals involving $\mathcal{H}(\mathbf{x},\mathbf{x}^*)$ must be evaluated in the CPV sense. This occurs in all considered problems.

Fig. 5.(a) shows the temperature distribution in the hollow cylinder. The solid line represents the analytical solution (Eq. (24)) whereas the markers show the numerical result obtained with the proposed method. Both results are in good agreement demonstrating the satisfactory performance of the procedure for computing this BIE. The temperature in the cylinder is plotted in Fig. 5.(b). The thermal gradient from the inner to the outer side is perfectly represented by the internal points.

3.2. Two-dimensional open acoustic domain with complex boundary geometry

Next, the capacity of the proposed method is analysed for solving the Helmholtz equation in an open boundary with complex geometry. In acoustics problems, u^i and t^i in Eq. (2) stand for the sound pressure and the particle normal velocity, respectively.

In this case, a two-dimensional six-petaled flower circumscribed between two circumferences of outer and inner radius 1 m and 0.25 m, respectively, was studied. The boundary geometry is shown in Fig. 6. Twelve patches were used to approximate the geometry by quadratic Bézier curves. The problem properties were fluid density $\rho = 1.225\,\text{kg/m}^3$ and sound propagation velocity $c_f = 340\,\text{m/s}$.

An incident pressure field given by $u^I(\mathbf{x}) = \exp(\imath\kappa\mathbf{d}\cdot\mathbf{x})$ was considered in this problem, with a polarized direction $\mathbf{d} = [1,1]$ (the unit imaginary number was denoted by the Greek letter $\imath$ to prevent confusion with some subscripts used in the paper). Dirichlet and Neumann conditions were prescribed on alternate petals so that the numerical solution provided the incident pressure field.

The Green's function in the frequency domain for sound pressure at receiver position $\mathbf{x}$ due to a harmonic source acting at $\mathbf{x}^*$ with frequency ω is:

$$\mathcal{G}(\mathbf{x},\mathbf{x}^*) = \frac{\imath}{4} H_0^{(1)}(\kappa r) \tag{26}$$

where $\kappa = \omega/c_f$ is the wavenumber, c_f is the sound propagation velocity, and $H_0^{(1)}$ is the Hankel function of the first kind. The Hankel function $H_0^{(1)}(\kappa r)$ has a logarithmic singularity given by its series

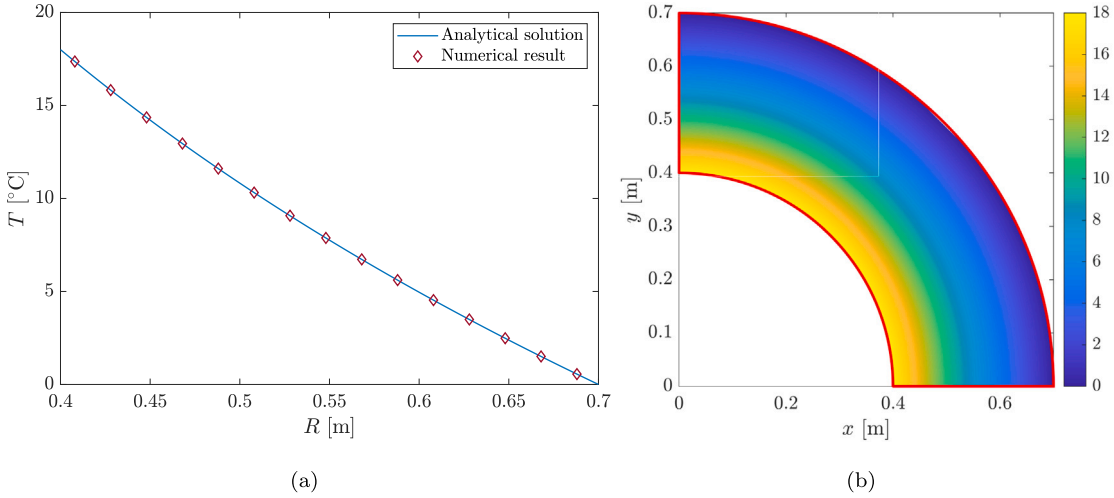

Fig. 5. Temperature profile [°C] in the hollow cylinder.

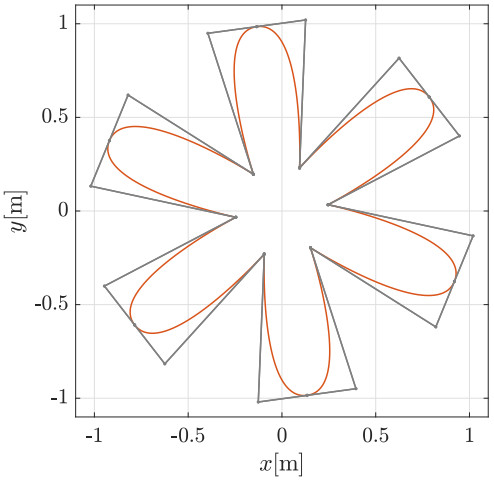

Fig. 6. Boundary geometry of a six-petal flower (red line) and their related control polygons (grey line). (For interpretation of the references to colour in this figure legend, the reader is referred to the web version of this article.)

expansion at zero:

$$\frac{\imath(2\log(\kappa r)+2\gamma-\imath\pi-2\log(2))}{\pi}+\mathcal{O}(\kappa r)^2 \tag{27}$$

where γ is the Euler–Mascheroni constant. This singularity is accurately integrated by the proposed approach.

Numerical results were compared with the reference solution $u^I(\mathbf{x})$ using the L_2 scaled error ϵ_2 to assess the accuracy. A convergence analysis was carried out for the element length given by $\kappa h = 3$ with successive $p-$enrichment. The element order was increased until convergence was reached. For this purpose, it was considered that the problem solution was properly approximated if the error satisfied $\log(\epsilon_2(h,p-1)/\epsilon_2(h,p+1)) \leq 1$. The L_2 scaled error ϵ_2 was evaluated over a grid of 378 internal points spaced a distance equal to the wavelength $(2\pi/\kappa)$ in both Cartesian directions. The problem solution was computed for: (i) $M = 3(p+1)$; (ii) $M = 4(p+1)$; and (iii) $M = 8(p+1)$.

Fig. 7.(a) shows the result of the convergence analysis. The convergence rate improved as the element order increased, with the lowest error $\mathcal{O}(10^{-5})$ being achieved for $p = 8$. The results of this analysis allow us to conclude that at least $M = 4(p+1)$ points are necessary in the BEM implementation to obtain accurate results.

The wave propagation over the unbounded domain is shown in Fig. 7.(b). The sound pressure does not present any discontinuity at the six-petal flower boundary according to the accuracy of the methodology.

3.3. Circular inclusion in two-dimensional elastostatics

In this section, a two-dimensional plane strain problem that couples two different boundaries is studied. Here, u^i and t^i in Eq. (2) represent the displacement and traction fields, respectively.

The geometry was composed of an annulus with a circular inclusion of different materials (see Fig. 8), introducing a discontinuity in the solution due to the interaction between both solids. The external side of the annulus was subjected to a unitary radial displacement. This benchmark is useful to test the representation of traction and displacement fields across a material interface [33].

Two subdomains were defined to represent this problem, ensuring the compatibility of displacements and the equilibrium of forces at the interface [34]. The first subdomain was a circle with radius $R_i = 3\,\text{m}$, Poisson ratio $\nu_i = 0.3$ and Young modulus $E_i = 10^4\,\text{Pa}$. The second subdomain consisted in an annulus with the same interior radius as the inner circle, and external radius $R_o = 15\,\text{m}$. The properties of this subdomain were Poisson ratio $\nu_o = 0.3$ and a Young modulus $E_o = 10^5\,\text{Pa}$.

Due to the symmetry of the problem, only a quarter of both boundaries were discretized. The first solid was introduced by Bézier curves: two linear patches for both symmetry axis, and one cubic patch for the circular shape. Meanwhile, the second solid needed four patches to be totally described as the boundary assessed in Section 3.1. The model was discretized into elements of order $p = 6$ with a maximum length of $h = 1\,\text{m}$.

Dirichlet and Neumann conditions were prescribed in the normal and tangential directions of the symmetry axis, respectively. Radial displacement $u_r(R_0) = 1\,\text{m}$ was also imposed at the external radius of the annulus.

This problem can be solved analytically leading to the following displacement field in polar coordinates [33]:

$$u_r(R)=\begin{cases}\left[\left(\dfrac{1}{R_o}-\dfrac{R_o}{R_i^2}\right)\alpha+\dfrac{R_o}{R_i^2}\right]R & \text{for} \quad 0\leq R\leq R_i\\ \left(\dfrac{R}{R_o}-\dfrac{R_o}{R}\right)\alpha+\dfrac{R_o}{R} & \text{for} \quad R_i\leq R\leq R_o\end{cases} \tag{28}$$

$$u_\theta = 0 \tag{29}$$

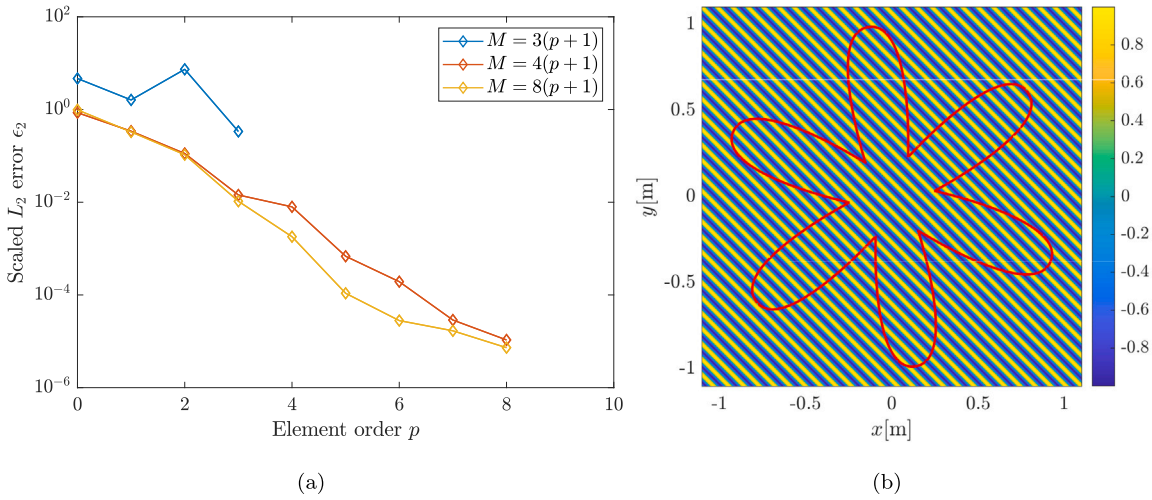

Fig. 7. (a) L_2 scaled error ϵ_2 for different number of points in the quadrature rule (M) depending on the element order. (b) Pressure field over the unbounded domain (the open boundary is represented in red line). (For interpretation of the references to colour in this figure legend, the reader is referred to the web version of this article.)

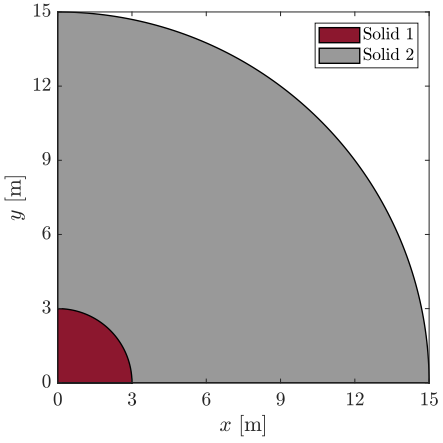

Fig. 8. Geometry of the subdomains.

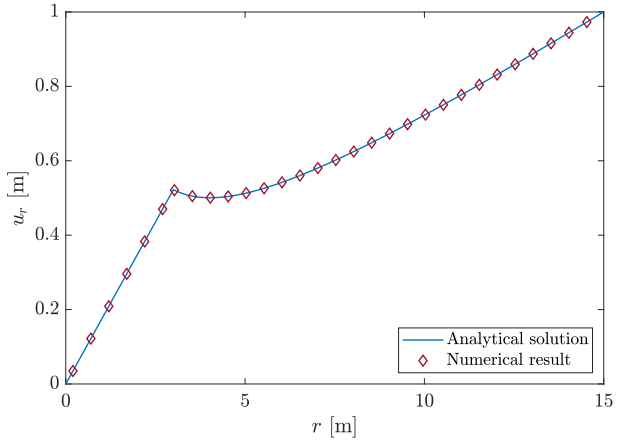

Fig. 9. Radial displacements along both subdomains. Comparison of computed results and the analytical solution.

with

$$\alpha = \frac{(\lambda_i + \mu_i + \mu_o)R_o^2}{(\lambda_o + \mu_o)R_i^2 + (\lambda_i + \mu_i)(R_o^2 - R_i^2) + \mu_o R_o^2} \tag{30}$$

where λ_i, λ_o, μ_i and μ_o are the Lamé parameters of both materials and R is the radial distance from the origin.

The Green's function for an isotropic material in plane strain gives the displacement in the k direction due to an unit load acting in the l direction [4]:

$$\mathcal{G}_{kl}(\mathbf{x}, \mathbf{x}^*) = \frac{1}{8\pi G(1-\nu)} \left[(3-4\nu) \log\left(\frac{1}{r}\right) \delta_{kl} + \frac{\partial r}{\partial x_k} \frac{\partial r}{\partial x_l} \right] \tag{31}$$

where G is the shear modulus, ν the Poisson ratio and δ_{kl} the Kronecker delta. The singularity is of the logarithmic form for displacement.

Fig. 9 compares the analytical solution and the numerical results obtained with the proposed method, showing again an excellent agreement and the versatility of this numerical approach.

3.4. Wave scattering in a three-dimensional elastic cylindrical cavity

Finally, the proposed method is applied to study an elastodynamic harmonic boundary value problem, consisting of an infinite length cylindrical cavity with radius 1 m in an unbounded elastic medium. The problem is longitudinally invariant in the z direction, which allows the problem solution in two-and-a-half dimensions (2.5D) as the superposition of 2D solutions with different longitudinal wavenumber κ_z [24,34]:

$$\mathbf{u}(\mathbf{x}, \omega) = \int_{-\infty}^{+\infty} \widetilde{\mathbf{u}}(\widetilde{\mathbf{x}}, \kappa_z, \omega) e^{-\imath \kappa_z z} \, d\kappa_z \tag{32}$$

where $\widetilde{\mathbf{u}}(\widetilde{\mathbf{x}}, \kappa_z, \omega)$ is the frequency–wavenumber representation of the displacement, $\mathbf{x} = \mathbf{x}(x, y, z)$ and $\widetilde{\mathbf{x}} = \mathbf{x}(x, y, 0)$.

The homogeneous elastic medium was characterized by a shear wave velocity $c_s = 150\,\text{m/s}$, dilatational wave velocity $c_p = 300\,\text{m/s}$, and density $\rho = 1800\,\text{kg/m}^3$. The cavity was subjected to a dilatational point load of unit amplitude applied at $\mathbf{x} = (-3, 0, 0)$ [35]. The problem solution was computed for a frequency range from 1 to 200 Hz, and a wavenumber range from 1 to 128 rad/m.

As in the previous examples, the circular shape was approximated by cubic Bézier curves. Four patches were used to define the whole boundary geometry. The patches were discretized into a number of boundary elements ensuring $\kappa_p h = 3$, and a nodal density per wavelength $d_\lambda = 2\pi p/\kappa_p h = 12$, where $\kappa_p = \omega/c_p$, h is the element size, and p is the element order.

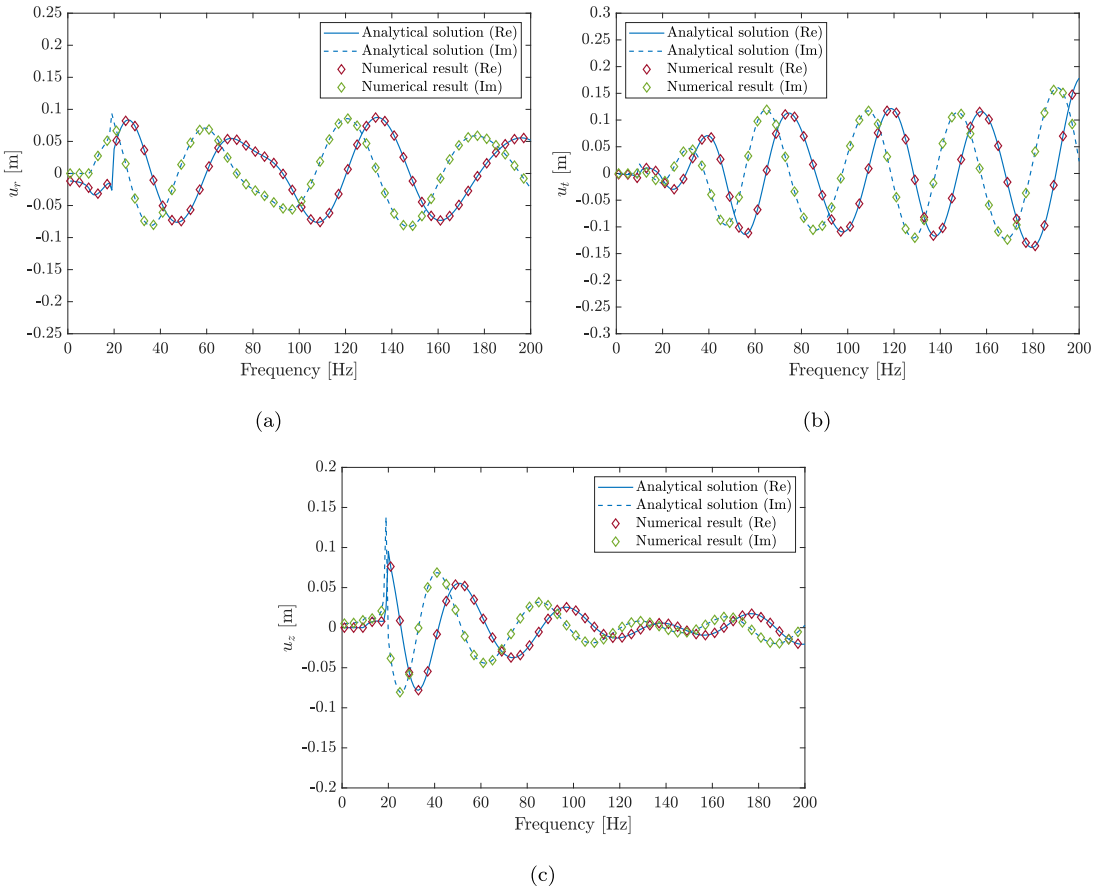

Fig. 10. (a) Radial, (b) tangential and (c) longitudinal displacements at $(0,3,0)$ due to a point source located at $(-3,0,0)$. Comparison of computed results and the analytical solution [36].

The two-and-a-half-dimensional Green's function is obtained by means of the potentials $\tilde{A}_p$ and $\tilde{A}_s$ for the irrotational and equivoluminal parts of the displacement vector, respectively [37]:

$$\tilde{A}_p = \frac{\iota}{4\rho\omega^2}\left[H_0^{(2)}(\kappa_\alpha r) - H_0^{(2)}(-\iota\kappa_z r)\right] \tag{33}$$

$$\tilde{A}_s = \frac{\iota}{4\rho\omega^2}\left[H_0^{(2)}(\kappa_\beta r) - H_0^{(2)}(-\iota\kappa_z r)\right] \tag{34}$$

being $\kappa_\alpha = \sqrt{\kappa_p^2 - \kappa_z^2}$ and $\kappa_\beta = \sqrt{\kappa_s^2 - \kappa_z^2}$, and κ_p and κ_s the wavenumbers for dilatational and shear waves, respectively. $H_0^{(2)}$ is the Hankel function of the second kind. Thus, the displacement $\mathcal{G}_{kl}(\mathbf{x},\mathbf{x}^*)$ in the k direction at $\mathbf{x}$ due to an unit harmonic load with frequency ω acting in the l direction at $\mathbf{x}^*$ for the wavenumber κ_z, is obtained from:

$$\mathcal{G}_{kl}(\mathbf{x},\mathbf{x}^*) = \frac{\partial^2(\tilde{A}_p - \tilde{A}_s)}{\partial x_k \partial x_l} + \delta_{kl}\bar{\nabla}^2\tilde{A}_s \tag{35}$$

The Hankel function $H_0^{(2)}(\kappa r)$ ($\kappa = \kappa_\alpha$ or $\kappa = \kappa_\beta$) has a logarithmic singularity, as in Section 3.2, given by its series expansion at zero:

$$-\frac{\iota(2\log(\kappa r) + 2\gamma + \iota\pi - 2\log(2))}{\pi} + \mathcal{O}(\kappa r)^2 \tag{36}$$

where γ is the Euler–Mascheroni constant.

Fig. 10 shows the radial, tangential, and longitudinal displacements at the observation point $\mathbf{x} = (0,3,0)$ for a longitudinal wavenumber $\kappa_z = 0.4\,\text{rad/m}$. The results computed by the proposed methodology are compared with the analytical solution available in Ref. [36]. The quadrature allows to compute the solution correctly. Moreover, Fig. 11 shows the x–component of the scattered wave field by the cylindrical cavity at a frequency $\omega = 1200\,\text{rad/s}$ ($f = 191\,\text{Hz}$). Displacements were normalized to $\bar{\mathbf{u}}(\mathbf{x},\omega) = \pi\mathbf{u}(\mathbf{x},\omega)c_s^2\rho r^*/(1\,\text{N})$, where r^* is the distance from the observation point to the source. The representation is limited to a half model, according to the problem symmetry. Maximum displacements were found at the source point and over the boundary. A shadow region was found behind the cavity where the displacement amplitude was considerably lower.

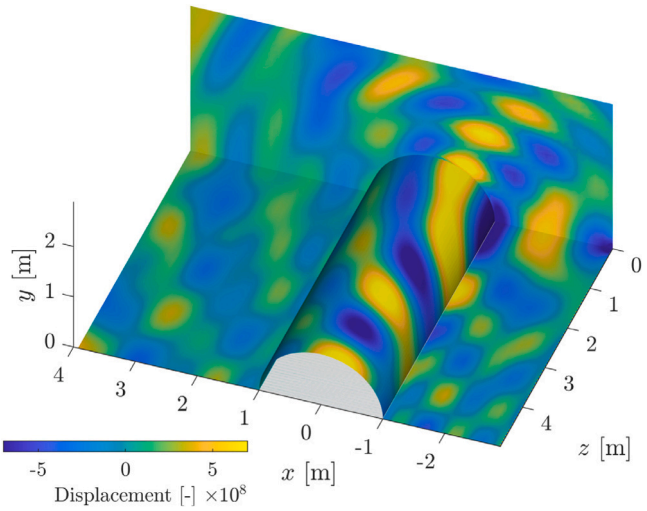

Fig. 11. Real part of the scattered wave field by a cylindrical cavity at $\omega = 1200\,\text{rad/s}$ ($f = 191\,\text{Hz}$).

4. Conclusions

This paper has proposed a novel quadrature that allows to compute the BIE by numerical integration. The methodology can be used for any element order and shape function. The BEM formulation, based on the Bézier–Bernstein space, has been considered to account for the exact boundary geometry and the use of arbitrary high-order elements. However, the approach can be easily implemented in any existing codes and to facilitate this task, a MATLAB script is provided as supplementary material.

The weights of the quadrature rule are given by the solution of an underdetermined system of equations in the minimum norm sense. The equations were obtained from the CPV of known integrals considering the shape functions of the elements used for the discretization. The accuracy of the proposed quadrature has been studied obtaining errors depending on the element order, that varied from $\mathcal{O}(10^{-15})$ for $p = 1$ to $\mathcal{O}(10^{-5})$ for $p = 20$.

The numerical performance of the methodology has been verified by the study of four problems involving different fundamental solutions: (*i*) heat transfer in a hollow cylinder; (*ii*) an open acoustic domain with a complex boundary geometry; (*iii*) the elastostatic behaviour of a annulus with an internal inclusion; and (*iv*) the wave scattering in a three-dimensional elastic cylindrical cavity. In all cases, the numerical results have been compared with analytical solutions obtaining a perfect agreement.

The proposed methodology allows to exploit the powerful and versatility of the BEM since the BIE is evaluated numerically. The work in progress includes the application of the proposed approach to others fundamental solutions.

CRediT authorship contribution statement

R. Velázquez-Mata: Methodology, Software, Investigation, Validation, Writing – original draft, Writing – review & editing. **A. Romero:** Conceptualization, Methodology, Software, Investigation, Validation, Funding acquisition, Supervision, Writing – original draft, Writing – review & editing. **J. Domínguez:** Conceptualization, Methodology, Investigation, Supervision, Writing – original draft, Writing – review & editing. **A. Tadeu:** Conceptualization, Methodology, Software, Investigation, Validation, Supervision, Writing – original draft, Writing – review & editing. **P. Galvín:** Conceptualization, Methodology, Software, Investigation, Validation, Funding acquisition, Supervision, Writing – original draft, Writing – review & editing.

Declaration of competing interest

The authors declare that they have no known competing financial interests or personal relationships that could have appeared to influence the work reported in this paper.

Acknowledgements

The authors would like to acknowledge the financial support provided by the Spanish Ministry of Science, Innovation and Universities under the research project PID2019-109622RB-C21; US-126491 funded by the FEDER Andalucía 2014–2020 Operational Program and the Andalusian Scientific Computing Centre (CICA).

Appendix A. Solution of generalized moments

The generalized moments are obtained according to the following formulas:

$$\int_{-1}^{1} B_k^n(\xi)\, d\xi = \int_0^1 B_k^n(t) \frac{d\xi}{dt}\, dt = \left[\frac{2}{n+1} \sum_{j=k+1}^{n+1} B_j^{n+1}(t) \right]_0^1 = \frac{2}{n+1} \tag{A.1}$$

$$\int_{-1}^{1} B_k^n(\xi) \log|\xi^* - \xi|\, d\xi = \int_0^1 B_k^n(t) \log|\xi^* - 2t + 1| \frac{d\xi}{dt}\, dt \tag{A.2}$$

$$\begin{aligned} \mathrm{CPV} \int_{-1}^{1} \frac{B_k^n(\xi)}{\xi^* - \xi}\, dt &= \mathrm{CPV} \int_0^1 \frac{B_k^n(t)}{\xi^* - 2t + 1} \frac{d\xi}{dt}\, dt \\ &= B_k^n(t^*)\, \mathrm{CPV} \int_0^1 \frac{1}{\xi^* - 2t + 1} \frac{d\xi}{dt}\, dt + \int_0^1 \frac{B_k^n(t) - B_k^n(t^*)}{\xi^* - 2t + 1} \frac{d\xi}{dt}\, dt \end{aligned} \tag{A.3}$$

where,

$$\mathrm{CPV} \int_0^1 \frac{1}{\xi^* - 2t + 1} \frac{d\xi}{dt}\, dt = \begin{cases} \log\left|\dfrac{\xi^* + 1}{1 - \xi^*}\right| & |\xi^*| \neq 1 \\ \pm \log(2) & \xi^* = \pm 1 \end{cases} \tag{A.4}$$

The logarithmic singularity (Eq. (A.2)) is integrated using an adaptive quadrature [38], and the regular integral in Eq. (A.3) is solve by a Gauss–Legendre quadrature of degree $(n + 1)$.

Appendix B. Supplementary data

Supplementary material related to this article can be found online at https://doi.org/10.1016/j.enganabound.2022.04.036.

References

[1] Cheng AH-D, Cheng DT. Heritage and early history of the boundary element method. Eng Anal Bound Elem 2005;29(3):268–302, URL https://www.sciencedirect.com/science/article/pii/S0955799705000020.

[2] Domínguez J. Boundary elements in dynamics. Computational Mechanics Publications and Elsevier Aplied Science; 1993.

[3] Guiggiani M. The evaluation of cauchy principal value integrals in the boundary element method—a review. Math Comput Modelling 1991;15(3):175–84, URL https://www.sciencedirect.com/science/article/pii/089571779190063D.

[4] Brebbia C, Domínguez J. Boundary elements. an introductory course. McGraw-Hill; 1989.

[5] Aliabadi MH, Hall WS, Phemister TG. Taylor expansions for singular kernels in the boundary element method. Internat J Numer Methods Engrg 1985;21(12):2221–36, URL https://onlinelibrary.wiley.com/doi/abs/10.1002/nme.1620211208.

[6] Guiggiani M, Gigante A. A general algorithm for multidimensional Cauchy principal value integrals in the boundary element method. J Appl Mech 1990;57(4):906–15. http://dx.doi.org/10.1115/1.2897660.

[7] Karami G, Derakhshan D. An efficient method to evaluate hypersingular and supersingular integrals in boundary integral equations analysis. Eng Anal Bound Elem 1999;23(4):317–26, URL https://www.sciencedirect.com/science/article/pii/S095579979800085X.

[8] Mukherjee S. CPV and HFP integrals and their applications in the boundary element method. Int J Solids Struct 2000;37(45):6623–34, URL https://www.sciencedirect.com/science/article/pii/S0020768399001730.

[9] Mukherjee S. Finite parts of singular and hypersingular integrals with irregular boundary source points. Eng Anal Bound Elem 2000;24(10):767–76, URL https://www.sciencedirect.com/science/article/pii/S095579970000059X.

[10] Mukherjee S, Mukherjee YX, Ye W. Cauchy principal values and finite parts of boundary integrals—revisited. Eng Anal Bound Elem 2005;29(9):844–9, URL https://www.sciencedirect.com/science/article/pii/S0955799705001177.

[11] Marshall JP, Richardson JD. A three-dimensional, p-version BEM: High-order refinement leveraged through regularization. Eng Anal Bound Elem 2021;122:13–20, URL https://www.sciencedirect.com/science/article/pii/S0955799720302575.

[12] Telles JCF. A self-adaptive co-ordinate transformation for efficient numerical evaluation of general boundary element integrals. Internat J Numer Methods Engrg 1987;24(5):959–73, URL https://onlinelibrary.wiley.com/doi/abs/10.1002/nme.1620240509.

[13] Monegato G. Numerical evaluation of hypersingular integrals. J Comput Appl Math 1994;50(1):9–31, URL https://www.sciencedirect.com/science/article/pii/0377042794902879.

[14] Diligenti M, Monegato G. Integral evaluation in the BEM solution of (hyper)singular integral equations. 2D problems on polygonal domains. J Comput Appl Math 1997;81(1):29–57, URL https://www.sciencedirect.com/science/article/pii/S0377042797000071.

[15] Monegato G, Scuderi L. Numerical integration of functions with boundary singularities. J Comput Appl Math 1999;112(1):201–14, URL https://www.sciencedirect.com/science/article/pii/S0377042799002307.

[16] Monegato G. Definitions, properties and applications of finite-part integrals. J Comput Appl Math 2009;229(2):425–39, URL https://www.sciencedirect.com/science/article/pii/S0377042708001635.

[17] Kolm P, Rokhlin V. Numerical quadratures for singular and hypersingular integrals. Comput Math Appl 2001;41(3):327–52, URL https://www.sciencedirect.com/science/article/pii/S0898122100002777.
[18] Carley M. Numerical quadratures for singular and hypersingular integrals in boundary element methods. SIAM J Sci Comput 2007;29(3):1207–16.
[19] Carley M. Numerical quadratures for near-singular and near-hypersingular integrals in boundary element methods. Math Proc R Ir Acad 2009;109A(1):49–60, URL http://www.jstor.org/stable/40656988.
[20] Boykov IV, Boikova AI, Ventsel ES. An approximate method for evaluating hypersingular integrals. Eng Anal Bound Elem 2006;30(9):799–807, URL https://www.sciencedirect.com/science/article/pii/S0955799706000592.
[21] Theotokoglou EE, Tsamasphyros G. A modified Gauss quadrature formula with special integration points for evaluation of Quasi-singular integrals. Eng Anal Bound Elem 2006;30(9):758–66, URL https://www.sciencedirect.com/science/article/pii/S0955799706000920.
[22] Tsamasphyros G, Theotokoglou EE. A quadrature formula for integrals with nearby singularities. Internat J Numer Methods Engrg 2006;67(8):1082–93, URL https://onlinelibrary.wiley.com/doi/abs/10.1002/nme.1649.
[23] Khan S, Zaman S, ul Islam S. Approximation of Cauchy-type singular integrals with high frequency Fourier kernel. Eng Anal Bound Elem 2021;130:209–19, URL https://www.sciencedirect.com/science/article/pii/S0955799721001478.
[24] Romero A, Galvín P, Cámara-Molina JC, Tadeu A. On the formulation of a BEM in the bézier–Bernstein space for the solution of Helmholtz equation. Appl Math Model 2019;74:301–19, URL https://www.sciencedirect.com/science/article/pii/S0307904X19302720.
[25] MATLAB. version 9.11.0.1837725 (R2021b). Natick, Massachusetts: The MathWorks Inc.; 2021.
[26] Patera AT. A spectral element method for fluid dynamics: Laminar flow in a channel expansion. J Comput Phys 1984;54(3):468–88, URL https://www.sciencedirect.com/science/article/pii/0021999184901281.
[27] Brandao MP. Improper integrals in theoretical aerodynamics - the problem revisited. AIAA J 1987;25(9):1258–60. http://dx.doi.org/10.2514/3.9775.
[28] Romero A, Galvín P, Tadeu A. An accurate treatment of non-homogeneous boundary conditions for development of the BEM. Eng Anal Bound Elem 2020;116:93–101, URL https://www.sciencedirect.com/science/article/pii/S095579972030117X.
[29] Ramshaw L. Blossoming: a connect-the-dots approach to splines. Digital Equipment Corporation SRC Report No. 19; 1987.
[30] Seidel H-P. An introduction to polar forms. IEEE Comput Graph Appl 1993;13(1):38–46.
[31] Farouki RT, Goodman TNT, Sauer T. Construction of orthogonal bases for polynomials in Bernstein form on triangular and simplex domains. Comput Aided Geom Design 2003;20(4):209–30, URL https://www.sciencedirect.com/science/article/pii/S0167839603000256.
[32] Tadeu A, Simões N, Branco F. Steady-state moisture diffusion in curved walls, in the absence of condensate flow, via the BEM: a practical civil engineering approach (glaser method). Build Environ 2003;38(5):677–88, URL https://www.sciencedirect.com/science/article/pii/S0360132302002081.
[33] Schröder J, Wick T, Reese S, Wriggers P, Müller R, Kollmannsberger S, et al. A selection of benchmark problems in solid mechanics and applied mathematics. Arch Comput Methods Eng 2021;28(2):713–51. http://dx.doi.org/10.1007/s11831-020-09477-3.
[34] Romero A, Tadeu A, Galvín P, António J. 2.5D coupled BEM–FEM used to model fluid and solid scattering wave. Internat J Numer Methods Engrg 2015;101(2):148–64, URL https://onlinelibrary.wiley.com/doi/abs/10.1002/nme.4801.
[35] Antonio J, Tadeu A. 3D scattering by multiple cylindrical cavities buried in an elastic formation. Eur J Mech A Solids 2001;20(3):367–83, URL https://www.sciencedirect.com/science/article/pii/S0997753800011268.
[36] Eringen A. Propagations of elastic waves generated by dynamical loads on a circular cavity. J Appl Mech 1960;28:218–22.
[37] Tadeu AJB, Kausel E. Green's functions for two-and-a-half-dimensional elastodynamic problems. J Eng Mech 2000;126(10):1093–7.
[38] Shampine LF. Vectorized adaptive quadrature in MATLAB. J Comput Appl Math 2008;211(2):131–40, URL https://www.sciencedirect.com/science/article/pii/S037704270600700X.